Atmospheric
Chemistry
and Physics

Impact of water uptake and mixing state on submicron particle deposition in the human respiratory tract (HRT) based on explicit hygroscopicity measurements at HRT-like conditions

Ruiqi Man[1], Zhijun Wu[1,2], Taomou Zong[1], Aristeidis Voliotis[3,4], Yanting Qiu[1], Johannes Größ[5],
Dominik van Pinxteren[5], Limin Zeng[1], Hartmut Herrmann[5], Alfred Wiedensohler[5], and Min Hu[1]

[1]State Key Joint Laboratory of Environmental Simulation and Pollution Control, College of Environmental
Sciences and Engineering, Peking University, 100871 Beijing, China
[2]Collaborative Innovation Center of Atmospheric Environment and Equipment Technology, Nanjing University
of Information Science and Technology, 210044 Nanjing, China
[3]National Centre for Atmospheric Science, Department of Earth and Environmental Science, School of Natural
Sciences, The University of Manchester, Oxford Road, M13 9PL Manchester, UK
[4]Centre for Atmospheric Science, Department of Earth and Environmental Science, School of Natural
Sciences, The University of Manchester, Oxford Road, M13 9PL Manchester, UK
[5]Leibniz Institute for Tropospheric Research, 04318 Leipzig, Germany

Correspondence: Zhijun Wu (zhijunwu@pku.edu.cn)

Abstract. Particle hygroscopicity plays a key role in determining the particle deposition in the human respiratory tract (HRT). In this study, the effects of hygroscopicity and mixing state on regional and total deposition doses on the basis of the particle number concentration for children, adults, and the elderly were quantified using the Multiple-Path Particle Dosimetry model, based on the size-resolved particle hygroscopicity measurements at HRT-like conditions (relative humidity $= 98\%$) performed in the North China Plain. The measured particle population with an external mixing state was dominated by hygroscopic particles (number fraction $= (91.5 \pm 5.7)\%$, mean $\pm$ standard deviation (SD); the same below). Particle hygroscopic growth in the HRT led to a reduction by around 24 % in the total doses of submicron particles for all age groups. Such a reduction was mainly caused by the growth of hygroscopic particles and was more pronounced in the pulmonary and tracheobronchial regions. Regardless of hygroscopicity, the elderly group of people had the highest total dose among three age groups, while children received the maximum total deposition rate. With 270 nm in diameter as the boundary, the total deposition doses of particles smaller than this diameter were overestimated, and those of larger particles were underestimated, assuming no particle hygroscopic growth in the HRT. From the perspective of the daily variation, the deposition rates of hygroscopic particles with an average of $(2.88 \pm 0.81) \times 10^9$ particles h^{-1} during the daytime were larger than those at night ($(2.32 \pm 0.24) \times 10^9$ particles h^{-1}). On the contrary, hydrophobic particles interpreted as freshly emitted soot and primary organic aerosols exhibited higher deposition rates at nighttime ($(3.39 \pm 1.34) \times 10^8$ particles h^{-1}) than those in the day ($(2.58 \pm 0.76) \times 10^8$ particles h^{-1}). The traffic emissions during the rush hours enhanced the deposition rate of hydrophobic particles. This work provides a more explicit assessment of the impact of hygroscopicity and mixing state on the deposition pattern of submicron particles in the HRT.

1 Introduction

Toxicological and epidemiological studies showed that ambient particles can result in declining life expectancy and rising premature mortality (Chen et al., 2013; Correia et al., 2013; Pope and Dockery, 2013; Dockery et al., 1993; Pope et al., 2009). Compared with coarse particles, submicron particles (i.e., particles with diameter $\leq 1\,\mu m$) have smaller sizes and larger specific surface areas, which tend to carry more toxic and harmful components and reach deeper into the human respiratory tract (HRT; Oberdorster, 2001). Inhaled particles deposit along the HRT, mainly by diffusion, sedimentation, impaction, and interception (L. Wang et al., 2018). The major deposition mechanism depends on the particle size and specific deposition location (Varghese and Gangamma, 2009). Unlike ambient environments, conditions in the HRT are warm and humid, where the relative humidity (RH) can be as high as 99.5 % (Hussein et al., 2013). The unique environment can alter the chemical and physical characteristics of inhaled particles, leading to variations in particle deposition distributions and doses. To accurately quantify the deposition pattern of submicron particles in the HRT, it is therefore critical to account for such potential transformations and characterize inhaled particle properties in the HRT.

Due to the experimental limitations of measuring inhaled particle number size distributions (PNSDs), regional doses in the HRT are typically estimated by means of mathematical models (Hofmann, 2011). The most widely used dosimetry models are the International Commission on Radiological Protection (ICRP, 1994) model and the Multiple-Path Particle Dosimetry (MPPD) model (Asgharian et al., 2001). Estimating the particle deposition fraction (DF) in these models is based on aerosol properties and the individual's physiological parameters. These available dosimetry models, however, fail to incorporate some critical particle characteristics, especially hygroscopicity (Ferron, 1977), which may cause variations in the particle size and, therefore, affect the deposition efficiency and pattern of particles in different lung regions.

To date, many studies have assessed the effects of hygroscopicity on ambient particle deposition in the HRT based on assumed values of the hygroscopic parameter (Kappa, κ) representing non-hygroscopic, nearly hydrophobic, and hygroscopic particles (Voliotis and Samara, 2018) or estimations by parametric methods (Ching and Kajino, 2018; Hussein et al., 2013; Mitsakou et al., 2007; Haddrell et al., 2015; Vu et al., 2018). However, it is well-known that continental aerosols typically show an external mixing state and size-dependent hygroscopicity (Zong et al., 2021). Thus, in order to capture the real and high-time-resolution features of ambient particles' hygroscopic growth in the HRT, direct particle hygroscopic growth measurements are a matter of necessity.

To our best knowledge, there are only limited studies exploring the impact of the hygroscopic growth of ambient particles on the particle deposition by direct hygroscopicity measurements. Moreover, hygroscopicity measurements

using the humidified tandem differential mobility analyzer (H-TDMA; Londahl et al., 2009; Farkas et al., 2022; Vu et al., 2015; Kristensson et al., 2013) or the differential aerosol sizing and hygroscopicity spectrometer probe (DASH-SP; Youn et al., 2016) in these studies were all conducted at relatively lower RH ($\sim 90\,\%$) compared to that in the HRT (RH $= 99.5\,\%$). For example, Farkas et al. (2022) modeled DFs of aerosol particles with four different diameters and studied the particles in their dry state and after their hygroscopic growth at RH $= 90\,\%$ using a H-TDMA. Youn et al. (2016) examined size-resolved hygroscopicity data by DASH-SP for particles sampled near mining and smelting operations to study the effects of particles' hygroscopic growth on the HRT deposition of toxic contaminants. It was further assumed that κ was independent of RH on the premise that the effective molar volume of the solute does not vary with RH. However, the presence of surface-active substances, slightly soluble substances and the co-condensation of semi-volatile soluble organic compounds can result in the humidity-dependent characteristic of κ (Wu et al., 2013; Wex et al., 2009; Topping and McFiggans, 2012). For instance, Liu et al. (2018) showed that κ could vary from about 0.1 at RH $<20\,\%$ to less than 0.05 when RH $\approx 90\,\%$ due to the non-ideal mixing of water with hydrophobic and hydrophilic organic components. Therefore, an explicit hygroscopicity measurement at HRT-like conditions will make the deposition estimation more accurate.

In this study, the size-resolved particle hygroscopicity derived from a high humidity tandem differential mobility analyzer (HH-TDMA) at HRT-like conditions (RH $= 98\,\%$) was first used to quantify the effects of both hygroscopicity and external mixing state on the particle deposition in the HRT using the MPPD model. The deposition doses of submicron particles were calculated in the head, tracheobronchial (TB), and pulmonary (P) regions in the HRT for different age groups. Furthermore, the diurnal variations in deposition rates of hygroscopic and hydrophobic particles were also calculated to provide an insight into the particle deposition linked to human activities.

2 Materials and methods

2.1 The sampling site and instruments

The field campaign was conducted from 8 June to 6 July in 2014 at an ecological park in the rural area of Wangdu County (38.666° N, 115.210° E) in the North China Plain, a polluted area with a high population density and strong primary emissions. The surroundings were wheat fields without significant industry emissions. A detailed description of the sampling site can be found in our previous study (Wu et al., 2017b). In brief, a HH-TDMA and a twin differential mobility particle sizer (TDMPS) were employed to measure the hygroscopic growth factor (HGF) of specific size particles at RH $= 98\,\%$ and the PNSDs of particles ranging

from 3 to 800 nm, respectively. Besides, NO and CO were monitored by NO_x chemiluminescence analyzer (42i-TLE, Thermo Fisher Scientific) and trace-level carbon monoxide analyzer (48iQ, Thermo Fisher Scientific), respectively (Chen et al., 2020). The black carbon (BC) mass concentrations were measured by Multi-Angle Absorption Photometer (MAAP, model 5012, Thermo Fisher Scientific; Wang et al., 2019). The OH radical was measured by laser-induced fluorescence (LIF; Tan et al., 2020).

2.2 Particle hygroscopic growth measurement

The HH-TDMA was designed to measure the aerosol hygroscopic growth at high RH (90 %–98 %), using the technique of a temperature-controlled water bath, which is able to hold the RH of aerosols and sheath flow stable for RH > 90 % (Hennig et al., 2005). The RH in the second differential mobility analyzer (DMA) reached an absolute accuracy of ± 1.2 % for 98 % and a long-term stability of ± 0.1 %–0.4 % of set point values (Hennig et al., 2005). More detailed information regarding the HH-TDMA system was provided by Bian et al. (2014) and Wu et al. (2017b). The HGF was defined as the ratio of the wet particle diameter at a given RH ($D_{P, wet}$) to the dry particle diameter for RH < 10 % ($D_{P, dry}$) as follows:

$$HGF = \frac{D_{P, wet}}{D_{P, dry}}, \tag{1}$$

The TDMAinv method developed by Gysel et al. (2009) was used to invert hygroscopicity data of settled diameter particles (30, 50, 100, 150, 200, and 250 nm) to HGFs of size-resolved particles and hygroscopic growth factor probability distribution function (GF-PDF) at RH = 98 % (Gysel et al., 2009). The HGF was then converted into the hygroscopic parameter (κ) according to the κ–Köhler theory, as follows (Petters and Kreidenweis, 2007):

$$\kappa = (HGF^3 - 1) \left(\frac{\exp\left(\frac{A}{D_{P, dry}} \cdot HGF \right)}{RH} - 1 \right), \tag{2}$$

$$A = \frac{4\sigma_{s/a} M_w}{RT\rho_w}, \tag{3}$$

where HGF and $D_{P, dry}$ are the HGF measured at 98 % RH by HH-TDMA and the dry particle diameter, respectively. $\sigma_{s/a}$ is the droplet surface tension (assumed to be that of pure water; $\sigma_{s/a} = 0.0728$ N m^{-2}). M_w is the molecular weight of water. ρ_w is the density of liquid water. R is the universal gas constant, and T is the absolute temperature.

The head region, or upper respiratory tract, includes the nasal cavities, the pharynx, and the larynx. In this study, the wet diameter of aerosols above the larynx was assumed to be equilibrated with ambient air conditions (Ching and Kajino, 2018) and therefore set to the average value during the sampling period ($T = 26$ °C, RH = 60 %). The TB and P regions

belong to the lower respiratory tract which were saturated with water vapor, and the temperature and RH inside were 37 °C and 99.5 %, respectively (Vu et al., 2015). The wet particle diameter in the HRT was estimated by using the variant of Eq. (2). Detailed information can be found in Farkas et al. (2022). It should be noticed that the inhaled particle was assumed to reach the equilibrium size immediately once particles enter into the HRT in this study. However, the hygroscopic growth rate of particles depends on the particle size, hygroscopicity, the ambient environment conditions (such as RH and temperature), and the residence time in the body (Ching and Kajino, 2018). A previous study pointed out that particles with $D_p = 100$ nm can reach the equilibrium size in a few seconds, while the equilibration timescale of particles with $D_p > 1$ μm turns to minutes (Ching and Kajino, 2018).

2.3 Total, hygroscopic, and hydrophobic particle number size distributions

The TDMPS includes two Hauke-type DMAs that have different effective center rod lengths which measure aerosol particles of 20–800 and 3–20 nm, respectively. The two condensation particle counters (CPCs) count particles downstream of the DMAs. Combining the counts from the two CPCs, the TDMPS can measure the PNSD of particles from 3 to 800 nm (electrical mobility diameter). The instrument principle and structure of TDMPS can be found in Birmili et al. (1999) and Wiedensohler et al. (2012). To match the particle size range in the MPPD model, the electrical mobility diameter was converted to the aerodynamic diameter by Eq. (4), as follows (Khlystov et al., 2004):

$$d_a = d_m \sqrt{\mathcal{X} \times \frac{\rho \times C_{c(dm)}}{C_{c(da)}}}, \tag{4}$$

where d_a and d_m is the particle aerodynamic diameter (nm) and electrical mobility diameter (nm), respectively. ρ is the particle density (1.5 g cm^{-3} in this study; Hu et al., 2012). $\mathcal{X}$ is the shape factor. C_c is the Cunningham slip correction factor for a certain diameter. Similar to other studies, the shape factor $\mathcal{X}$ is assumed as 1, and C_c is neglected in the calculation (Khlystov et al., 2004; Hu et al., 2012). Therefore, the electrical mobility diameter (in the range of 10.3–756.6 nm) was converted to the aerodynamic diameter (in the range of 12.6–926.6 nm).

Taking the particle mixing state into account, the particle population can be categorized into hygroscopic and hydrophobic groups according to HGFs measured at RH = 98 % by HH-TDMA. Particles with HGF < 1.2 were regarded as hydrophobic particles, whereas those with HGF ≥ 1.2 were regarded as hygroscopic particles (X. Wang et al., 2018; Zong et al., 2021). The hydrophobic particles in urban environments have been interpreted as originating from freshly emitted soot and vehicle exhaust, while the hygroscopic particles have been regarded as experienc-

ing long-distance transport (Swietlicki et al., 2008; Baltensperger, 2002). To obtain the PNSDs for both groups, the total PNSD measured by TDMPS were scaled by the number fractions (NFs) of hydrophobic and hygroscopic particles. With HGF = 1.2 as the cutoff point, the GF-PDF for each selected size was divided into the hydrophobic and hygroscopic modes. The calculation methods of the HGF and NF of each mode were detailed in Zong et al. (2021). The NFs of size-resolved particles within the measuring range of the TDMPS were calculated by the linear interpolation methods, while those of particles out of the range were equal to the closest known NF.

2.4   Particle dose estimation

The MPPD model (version 3.04) was used to estimate the deposition of particles in the HRT, since it fits with the measured data better than the ICRP model (Londahl et al., 2007). This model calculates the deposition and clearance of monodisperse and polydisperse aerosols in the size range of 1 nm–100 µm in the respiratory tracts of laboratory animals, human adults, and children. Within each airway, the deposition is calculated using theoretically derived efficiencies for deposition by diffusion, sedimentation, impaction, and interception within the airway or airway bifurcation (Asgharian et al., 2001). The model requires the following parameters as input: (1) airway morphometry parameters (airway morphometry model, functional residual capacity (FRC), and upper respiratory tract (URT) volume), (2) particle properties (density and diameter), (3) exposure scenario (breathing frequency (BF) and tidal volume (TV)), and (4) deposition/clearance.

In this study, the stochastic model (60th percentile) was chosen, which is closer to the realistic structure of human lungs (Voliotis and Samara, 2018; Li et al., 2016; Asgharian et al., 2001; Wang et al., 2021; Lyu et al., 2018; Avino et al., 2018; Manigrasso et al., 2015). The particle diameter range was set as 0.01–10.0 µm. Particle density was taken as 1.5 g cm^{-3}, according to a previous study in Beijing (Hu et al., 2012). In order to obtain the deposition pattern of different age groups, the population was divided into three groups on the basis of their age, i.e., children (7–12 years old), adults (18–26 years old), and the elderly (>59 years old). Then, the particle deposition was estimated based on Chinese localized physiological parameters (Table 1). These values were considered for an exposure scenario for resting (e.g., sitting) and nasal breathing. All the model simulations were conducted based on this exposure scenario, using the male physiological parameters, as corresponding data for females were not available. Elsewhere it was shown that males received higher doses compared to females in all age classes due to the different physiological parameters (e.g., higher TV and FRC; Voliotis and Samara, 2018); hence, similar behavior would have been expected here. It should be noticed that the exposure time data came from the statistical results of the questionnaire survey of the outdoor activity time for the rural population in Hebei, China. While people may rest, take light exercise, or take heavy exercise during the exposure time, different exercise levels (e.g., sitting, walking, and exercising) can result in different dose estimations and are not discussed here. For instance, previous studies found that the exercise level had great impact on the minute ventilation and led to the increasing deposition dose (Londahl et al., 2007). All the other model input parameters were set as default. It should be noted that any clearance mechanisms were not considered in this study; hence, our results show the upper limit of exposure.

The DF is the ratio of the mass/number/surface area of the deposited particles to that of inhaled particles in a given region. The DFs of hygroscopic and hydrophobic particles considering hygroscopicity (hereinafter referred to as wet particles) were obtained based on the DFs of particles without considering hygroscopicity (hereinafter referred to as dry particles). More specifically, it is considered that the DF of wet particles with D_p after hygroscopic growth was equal to that of dry particles with the same diameter (D_p). Therefore, the DF curve of wet particles corresponds to shifting the particle size range of the DF curve of dry particles to the right. The daily particle number doses and deposition rates for size-resolved particles in a specific region were calculated as follows (Voliotis and Samara, 2018):

$$\text{Dose}_i = \text{DF}_i \times \text{PNC}_i \times \text{TV} \times \text{BF} \times t \qquad (5)$$
$$\text{Rate}_i = \text{DF}_i \times \text{PNC}_i \times \text{TV} \times \text{BF}, \qquad (6)$$

where Dose$_i$ is the deposition dose of ith size particle (particles d^{-1}), Rate$_i$ is the deposition rate of ith size particle (particles h^{-1}), DF$_i$ is the deposition fraction of ith size channel in a specific region, PNC$_i$ is the particle number concentration (cm^{-3}) corresponding to the ith size channel, TV is the tidal volume (mL), BF is the breathing frequency (min^{-1}), and t is the exposure time in ambient air (min d^{-1}). The deposition dose of a specific region was calculated by adding together doses of size-resolved particles, and the total dose was the sum of three regional doses. The dose without considering hygroscopicity was calculated on the basis of the dry PNSD. The dose considering hygroscopicity was the sum of particle doses of hygroscopic and hydrophobic groups, which was, respectively, calculated by the PNSDs of two groups.

3   Results and discussion

3.1   Particle number size distributions in the human respiratory tract

As described in Sect. 2.3, particles were categorized into hygroscopic and hydrophobic groups, according to their hygroscopicity at RH = 98 %. The hygroscopicity of size-resolved particles measured by HH-TDMA during the sampling period was displayed in Table S1. Figure 1 showed the

Table 1. Physiological and breathing parameters for three age groups.

Age groups[a]	FRC (mL)	Height[e] (cm)	URT volume[f] (mL)	TV[e] (mL)	BF[e] (min^{-1})	Exposure time ($min\,d^{-1}$)
Children	1330[b,c]	139.3	21.91	630	22	96[g]
Adults	3338[d]	158.5	36.31	730	18	253[h]
Elderly people	3259[d]	166.9	34.01	760	18	241[h]

[a] Based on the available data, age groups here refer to males. [b] Due to the lack of data, the FRC value of children is not a Chinese localization parameter. [c] Stocks and Quanjer (1995). [d] Cao (2009). [e] Zhu (2006). [f] Hart et al. (1963). [g] Duan (2016). [h] Duan et al. (2014).

average ambient PNSD under dry conditions (RH <30 %) over the entire field campaign and those of hygroscopic and hydrophobic particles in the HRT. The wet diameters of hydrophobic and hygroscopic particles in the HRT were shown in Table S2. The average particle number concentrations (PNCs) of hygroscopic and hydrophobic particles were $(1.76 \pm 1.64) \times 10^4$ (mean ± standard deviation (SD); the same below) and $(1.70 \pm 3.14) \times 10^3\,cm^{-3}$, respectively. The hygroscopic particles accounted for an average of (91.5 ± 5.7) % of the total PNCs and dominated the measured aerosol population. The PNSDs of ambient aerosols during the daytime and nighttime are shown in Fig. S1.

As shown in Fig. 1b, hygroscopic particles grew slightly in the head (the blue line), while they had a remarkable growth in the TB and P regions (the red line) attributed to high humidity conditions and water uptake. Particularly, the diameter of hygroscopic particles corresponding to the maximum PNC shifted from about 90 to 250 nm. As expected, no obvious size growth of hydrophobic particles took place in the three regions in the HRT, and the peak appeared at $D_p \approx 40\,nm$ (Fig. 1c).

3.2 Regional and total deposition fractions

Taking the adult group as an example, size-resolved regional and total DFs of particles under dry conditions (black dots) and hydrophobic (blue dots) and hygroscopic (red dots) particles in humid environments are shown in Fig. 2. The size-resolved DFs for children and the elderly are shown in Figs. S2–S3. As shown in the three figures, the regional and total DFs of all age groups, respectively, followed the same trends regardless of particle hygroscopicity. Due to the similar physiological parameters (such as the FRC, URT volume, TV, and BF, as shown in Table 1) of adults (Fig. 2) and the elderly (Fig. S3), their regional and total DF functions were similar to each other. While, for the reason that the FRC is positively correlated with body weight, the FRC of children was nearly one-third of that of adults and the elderly, which may lead to the different DF curves of children (Fig. S2). Compared with adults and the elderly, children had lower DFs of ultrafine particles in the head and higher DFs of submicron particles in the P region, resulting in higher total DFs of submicron particles.

As shown in Fig. 2a, there was no significant difference between head DFs, regardless of whether hygroscopicity was considered or not, because the conditions within the upper respiratory tract were in balance with the surrounding environment (Ching and Kajino, 2018). With the increasing D_p, the head DFs decreased first and reached the minimum at around 150 nm, then increased sharply, which is similar to the trend of the head DF curve using the MPPD by Youn et al. (2016).

In the TB, the DF declined monotonically with the increasing particle diameter, and tended to plateau for particles with $D_p > \sim 100\,nm$ (Fig. 2b), which is consistent with the results of previous studies (Youn et al., 2016; Hussein et al., 2019; Varghese and Gangamma, 2009). If hygroscopicity was not taken into consideration, DFs of submicron particles were overestimated for both groups (i.e., the blue dots for hydrophobic particles and the red dots for hygroscopic particles). Using the percentage of the difference between DFs in two cases (i.e., considering hygroscopicity or not) and the DF without considering hygroscopicity as a weight, tracheobronchial DFs of hydrophobic particles were overestimated by less than 9.7 %, while they were 23.0 % on average for hygroscopic particles. For example, the DF of particles with dry diameters at around 50 nm was 0.131 without considering hygroscopicity, and it shifted to 0.120 for hydrophobic particles and 0.083 for hygroscopic particles considering hygroscopicity, with the differences of 8.4 % and 36.6 %.

Compared with size-resolved DFs of particles under dry conditions (the black dots in Fig. 2c), the DFs of hydrophobic (the blue dots) and hygroscopic (the red dots) particles in the P region were overestimated in the range of 20–500 and 20–250 nm, respectively, and those of the particles outside the above diameter ranges were underestimated. The DFs of hydrophobic and hygroscopic particles were, respectively, overestimated (underestimated) by up to 14.1 % (10.7 %) and 53.1 % (109.7 %). Similarly, taking particles with a dry particle diameter of 50 nm as an example, the DF in the P was 0.250 without considering hygroscopicity, while it reduced to 0.133 (0.228) for hygroscopic (hydrophobic) particles considering hygroscopicity. Besides, our results resembled the results of Youn et al. (2016) and Varghese and Gangamma (2009), as there was only one peak at the DF curve of the P region in the submicron range without considering hygroscopicity (black dots). Considering hygroscopic-
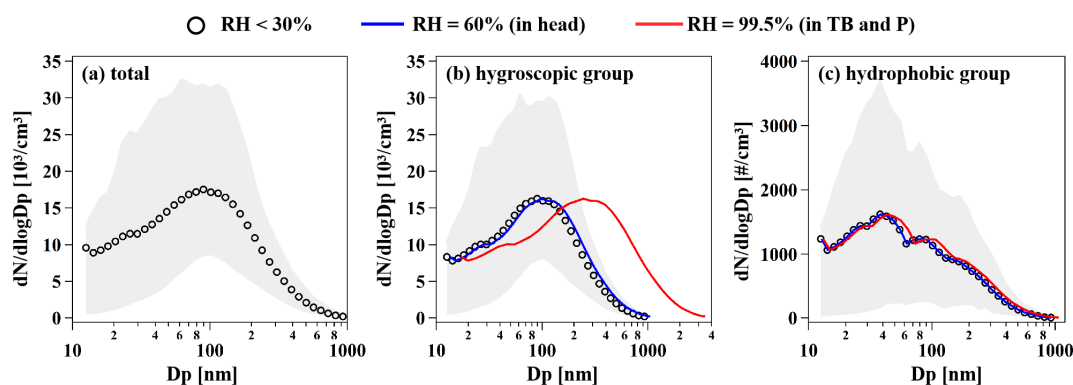
Figure 1. (a) The average particle number size distribution (PNSD) measured by TDMPS during the sampling period. The average PNSDs of **(b)** hygroscopic and **(c)** hydrophobic groups in the human respiratory tract at different relative humidities (RHs). The black markers, blue lines, and red lines represent PNSDs under dry conditions (RH <30 %), in the head (RH = 60 %), and in the TB and P (RH = 99.5 %), respectively. The upper and lower edges of the gray area represent the 90th and 10th quantiles of PNSDs, respectively.
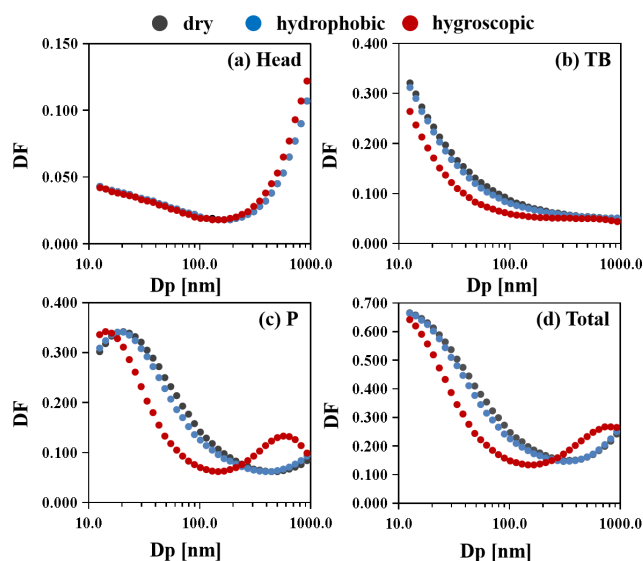
Figure 2. Size-resolved **(a)** head, **(b)** TB, **(c)** P, and **(d)** total deposition fractions (DFs) of particles under dry conditions (i.e., without considering hygroscopicity) and hydrophobic and hygroscopic particles in humid environments (i.e., considering hygroscopicity) for the adult group. For clarity, the abscissa of Fig. 2 refers to the dry diameter of particles. The black, blue, and red dots represent dry, hydrophobic, and hygroscopic particles, respectively. In Fig. 2a, the black dots representing DFs under dry conditions are hidden behind the blue dots representing DFs of hydrophobic particles because these two sets of DFs are close to each other.

ity, another peak of larger hygroscopic particles ($\sim$ 800 nm) appeared. This indicates that particle hygroscopicity enables more submicron particles with relatively large diameters to deposit in the deepest parts of the lung. It should be noted that the particle density would change during hygroscopic growth, which was not considered in the calculation due to the lack of measurements of the particle density. The sensi-

tivity analysis of the particle density on the regional DFs is shown in Fig. S4.

In Fig. 2d, the total DFs of hydrophobic particles (the blue dots) had a similar trend to those of dry particles due to regional DFs mentioned above. For the hygroscopic group (the red dots), with $D_p = 270$ nm as the boundary, DFs of smaller particles were overestimated by 27.6 % on average, while those of larger particles were underestimated by 28.6 % on average. When considering hygroscopicity, submicron particles undergo hygroscopic growth by water uptake, and particle sizes increase as a whole (Fig. 1b and c). For small particles dominated by diffusion, as D_p increases, the Brownian motion intensity decreased and the diffusion deposition decreased accordingly. For large particles dominated by interception and inertial impaction, these two efficiencies increased with the particle size. Therefore, the corresponding particle deposition increased. This result is consistent with the previous study using the ICRP model, which concluded that the deposition of particles with $D_p < 200$ nm was overestimated without considering water uptake (Vu et al., 2015). Additionally, the trend of the total DFs in both cases in this study is similar to the experimental data of breathing NaCl with/without hygroscopicity through the nose (Chalvatzaki and Lazaridis, 2018). In general, hygroscopicity has a significant effect on regional DFs of hygroscopic particles in the TB and P regions, while no obvious variation occurred in the DFs of two groups in the head or those of hydrophobic particles in the TB and P.
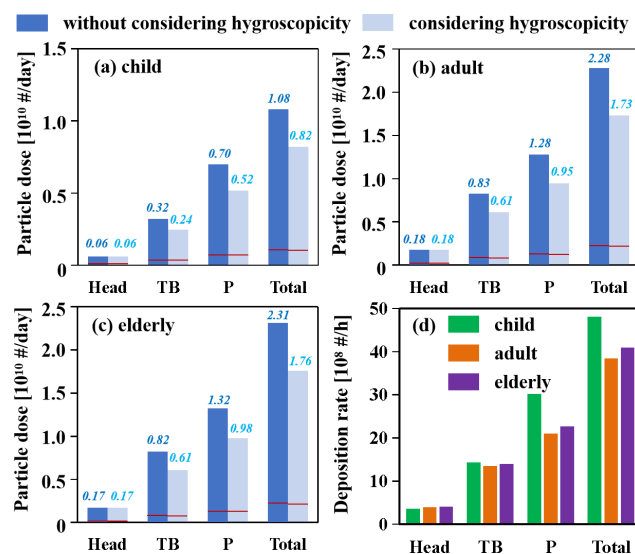
3.3 Regional and total deposition doses and rates for different age groups

Regional (head, TB, and P) and total deposition number doses with/without considering hygroscopicity were calculated for children (a), adults (b), and the elderly (c) in Fig. 3. Specific values of deposition doses of hydrophobic and hygroscopic particles in two cases can be found in Ta-

bles S3–S5. Hussein et al. (2013) found that the deposited dose calculations in the other age groups (the elderly and teenagers) were of the same order of magnitude as that of adults. This is also true in our results. In both cases, the elderly group had the highest total deposition dose among the three groups, followed by adults and children, while Voliotis and Samara (2018) concluded that adults received the highest doses among all age groups, which may be caused by different physiological parameter values, such as the TV. In each group, the contribution of the P region to the total dose was the greatest (> ∼ 55 %), which was similar to the published conclusions found elsewhere (Voliotis and Samara, 2018; Hussein et al., 2013; Manigrasso et al., 2017; Li et al., 2016). Moreover, the proportion of pulmonary deposition in total doses for children was up to 62.9 % when considering hygroscopicity. By comparison, it accounted for 54.6 % and 55.7 % for adults and the elderly, respectively. This indicates that particles inhaled by children are more likely to deposit in their pulmonary regions, which is in accordance with the results of previous studies (Voliotis and Samara, 2018; Voliotis et al., 2021). Taking hygroscopicity into consideration, total deposition doses significantly reduced by about a quarter (24.0 %–24.1 %) for all age groups. The greatest reduction took place in doses in the P region (25.9 %–26.3 %), followed by doses in the TB (24.2 %–26.1 %). Head deposition had only minor variations (−0.9 % to +0.5 %) in both cases.

In both cases, adults (Fig. 3b) and the elderly (Fig. 3c) received similar regional and total doses. In contrast, children had the minimum total dose (Fig. 3a), which was around half (47.4 % on average) of that for adults. As shown in Eq. (5), the exposure time is an important parameter for deposition dose calculations. The exposure time of adults and the elderly was more than twice than that of children (Table 1), which resulted in the greater deposition dose for the former two groups. Therefore, to remove the impact of the exposure time, the regional and total deposition rates for three age groups were also calculated and are shown in Fig. 3d. Children received the maximum total deposition rate ($(4.81 \pm 4.55) \times 10^9$ particles h^{-1}), followed by the elderly ($(4.09 \pm 3.92) \times 10^9$ particles h^{-1}), and adults received the minimum ($(3.84 \pm 3.69) \times 10^9$ particles h^{-1}). The regional deposition rate in the TB and P regions for the three age groups showed the same order as the total deposition rate, while the order in the head was quite different. Specifically, the three age groups had a similar deposition rate in the head.

As shown by the red lines in Fig. 3, the contribution of hydrophobic particles to total deposition doses was about 10.0 % for all age groups, while it increased to 12.5 % after considering hygroscopicity. Hydrophobic particles were assumed to originate from freshly emitted soot and exhaust (Swietlicki et al., 2008; Baltensperger, 2002), which are composed of species that do great harm to human health, such as BC (Highwood and Kinnersley, 2006), primary organic aerosols (Mauderly and Chow, 2008), and polycyclic aromatic hydrocarbons (Kim et al., 2013; Haritash and Kaushik,

Figure 3. Regional and total deposition doses for **(a)** children, **(b)** adults, and **(c)** the elderly with/without considering particle hygroscopicity. The dark blue columns represent doses without considering hygroscopicity. The light blue columns represent doses considering hygroscopicity. The red lines on the column represent the division of doses of hygroscopic (above the red line) and hydrophobic particles (below the red line). Numbers above each column mean the corresponding particle doses with a unit of 10^{10} particles d^{-1}. **(d)** The average regional and total deposition rates considering hygroscopicity for three age groups. The green, orange, and purple columns represent children, adults, and the elderly, respectively.

2009). Therefore, we need to pay attention to the deposition effects of hydrophobic particles.

The adults' regional and total deposition doses of size-resolved particles with/without considering hygroscopicity are shown in Fig. 4. The effects of hygroscopicity in particle doses in the head (Fig. 4a) are insignificant because the RH in the upper respiratory tract was close to that under dry conditions. Regional doses in the TB decreased due to particle hygroscopic growth (Fig. 4b), and the greatest reduction (∼ 33 %) appeared between 40 and 80 nm in diameter. Similarly, particle hygroscopicity considerably decreased deposition doses (up to 50.3 %) in the P region for particle sizes between 20 and 240 nm (Fig. 4c). Inversely, particle doses increased (up to 102.6 %) in the P region for diameters less than 20 and above 240 nm due to hygroscopic growth. As a result, the total deposition dose, as shown in Fig. 4d, was overestimated for particles smaller than around 270 nm, with a maximum of 40.8 % without considering hygroscopicity. The deposition doses of particles larger than this diameter were underestimated, and the maximum was 43.0 %.
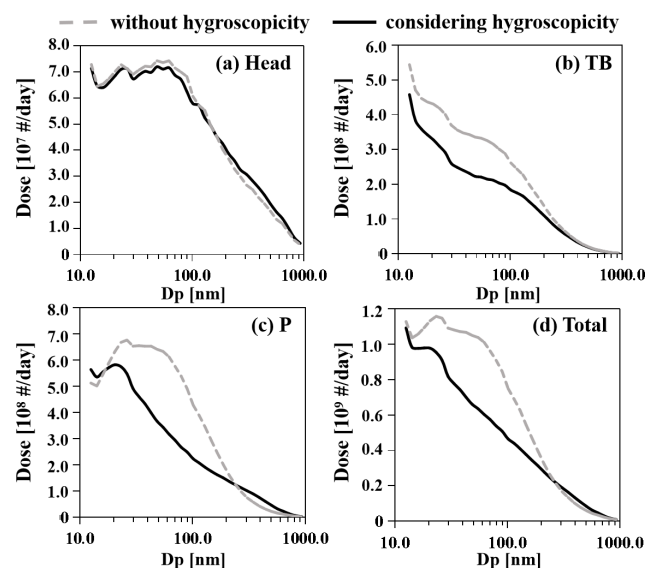
Figure 4. (a) Head, **(b)** TB, **(c)** P, and **(d)** total deposition doses of size-resolved particles for adults with/without considering hygroscopicity. For clarity, the abscissa of Fig. 4 refers to the dry diameter of particles. The gray dashed line represents doses without considering hygroscopicity. The black solid line represents doses considering hygroscopicity.

3.4 Deposition rates of hygroscopic and hydrophobic particles

In order to link human daily activities to the particulate matter deposition, the diurnal variations in deposition rates of hygroscopic and hydrophobic particles considering hygroscopicity for the adult group averaged over the entire field campaign were investigated and are displayed in Fig. 5. Additionally, the average concentrations of NO, CO, BC, and OH radicals are also given in Fig. 5. By comparison, the diurnal variations in the deposition rates of hygroscopic and hydrophobic particles without considering hygroscopicity are displayed in Fig. S5. No matter which time was considered during a day, the deposition rate of hygroscopic particles $((3.60 \pm 6.68) \times 10^9$ particles h^{-1}) in the HRT was nearly 1 order of magnitude higher than that of hydrophobic particles $((5.15 \pm 14.4) \times 10^8$ particles h^{-1}).

The deposition rate of hygroscopic particles (Fig. 5a) was higher during the daytime (05:00–19:00 local time (LT; UTC+8); $(2.88 \pm 0.81) \times 10^9$ particles h^{-1}) than at night (from 20:00 to 04:00 LT on the next day; $(2.32 \pm 0.24) \times 10^9$ particles h^{-1}). The peak appeared at noon, and the deposition rate reached the top at 12:00 LT $(4.74 \times 10^9$ particles h^{-1} on average). The enhanced deposition rate can be attributed to the strong atmospheric oxidation capacity during the daytime, indicated by OH radical in Fig. 5c, which creates new particles or transfers the pre-existing aerosols to more aged particles through nucleation, semi-volatile partitioning, and multiphase chemistry

(Raes et al., 2000; Donahue et al., 2014; Tan et al., 2020; Rudich et al., 2007). For instance, a previous study pointed out that the atmospheric oxidation capacity may enhance the particle formation by oxidizing the trace gases emitted from sources (such as biomass burning) and producing low-volatility condensable vapors which nucleate in the plume (Wu et al., 2017a). Therefore, the ultrafine particles may be produced during transport (Wu et al., 2017a). During the field campaign, the new particle formation (NPF) events took place frequently (Fig. S6). Our previous study showed that the NPF events and subsequent growth produced a large amount of hygroscopic and internally mixed particles (Wu et al., 2017b), thus increasing the PNC (as shown in the black line in Fig. 5a) and leading to the enhanced deposition rate of hygroscopic particles during the day. It is indicated that the deposition rates of particles were mainly influenced by the PNC.

On the contrary, hydrophobic particles (Fig. 5b) exhibited a higher deposition rate at nighttime $((3.39 \pm 1.34) \times 10^8$ particles h^{-1}) than that during the day $((2.58 \pm 0.76) \times 10^8$ particles h^{-1}). The deposition rate of hydrophobic particles peaked at 06:00–08:00 LT during morning rush hours $(3.37 \times 10^8$ particles h^{-1} on average), as indicated by NO, CO, and BC concentrations in Fig. 5c. In the evening, the deposition rate increased step-wise and reached the maximum $(5.17 \times 10^8$ particles h^{-1} on average) at around 21:00 LT. Correspondingly, BC concentrations increased as well. The strong primary emissions (such as the biomass burning process (Wu et al., 2017a)), weak chemical processes, and low boundary layer height (Zhang et al., 2014) resulted in the increased hydrophobic particle number concentration. Thus, people who are exposed to outdoor air during rush hours and in the evening may have a higher exposure risk to hydrophobic particles.

4 Conclusions and implications

To accurately quantify the effects of both hygroscopicity and the external mixing state on the particle deposition, the size-resolved particle hygroscopicity measured at HRT-like conditions (RH = 98 %) was used to estimate the deposition doses of submicron particles in the HRT for different age groups with/without considering hygroscopicity by using the MPPD model.

The total particle number concentrations were dominated by hygroscopic particles (number fraction = (91.5 ± 5.7) %). Taking hygroscopicity into consideration, total deposition doses significantly reduced by about a quarter (24.0 %–24.1 %) for all age groups. The greatest reduction took place in doses in the P (25.9 %–26.3 %) and TB (24.2 %–26.1 %) regions. Head deposition had only minor variations (−0.9 % to +0.5 %) in both cases. With 270 nm as the boundary, the total doses of smaller particles were overestimated, and those of larger particles were underestimated. Regardless of
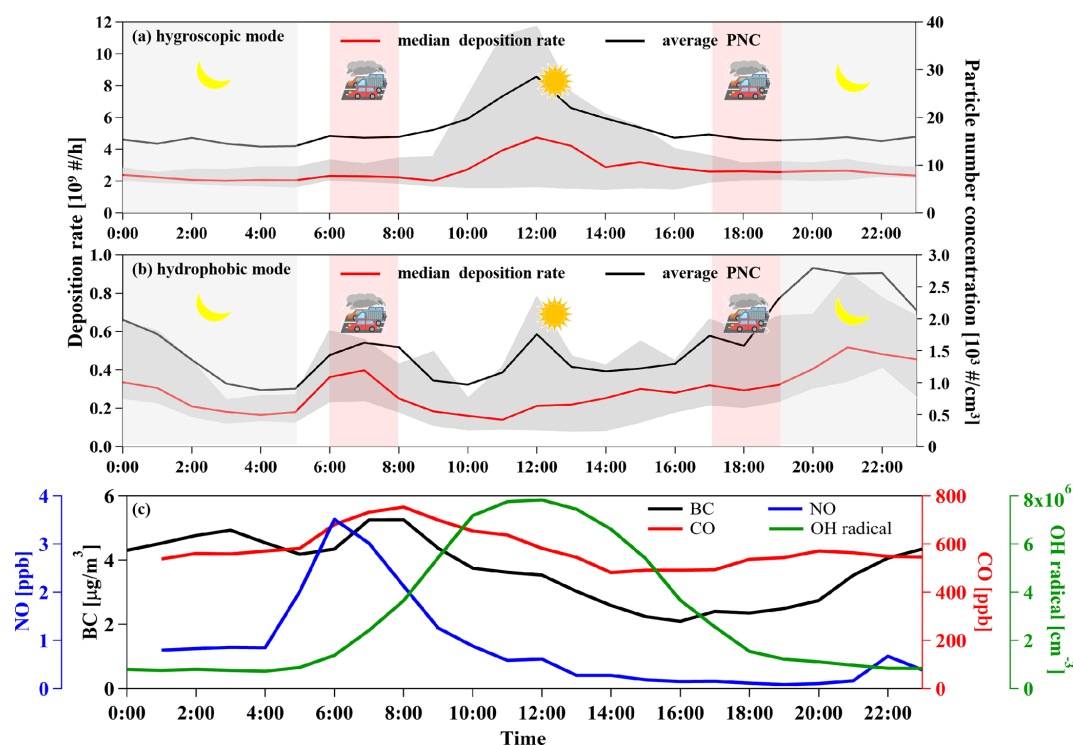
Figure 5. The diurnal variations in deposition rates considering hygroscopicity and particle number concentrations (PNCs) of **(a)** hygroscopic and **(b)** hydrophobic particles for adults. The red lines represent the median deposition rate. The upper and lower edges of the gray area represent the 75th and 25th quantiles of deposition rates, respectively. The black lines represent the average PNC. **(c)** The diurnal variations in the average concentrations of NO, CO, BC, and OH radicals during the sampling period. The blue, red, black, and green lines represent NO, CO, BC, and OH radicals, respectively.

hygroscopicity, the elderly group received the highest total doses, and children had the lowest doses, which was around half of that for the elderly. Pulmonary doses dominated the deposition pattern. When it comes to the deposition rate, children received the maximum total deposition rate, followed by the elderly group, and adults received the minimum. The diurnal variations in deposition rates of hygroscopic and hydrophobic particles were also calculated. The deposition rate of hygroscopic particles was higher during the daytime ($(2.88 \pm 0.81) \times 10^9$ particles h^{-1} vs. $(2.32 \pm 0.24) \times 10^9$ particles h^{-1} at night), which is attributed to the strong atmospheric oxidation capacity. Hydrophobic particles exhibited a higher deposition rate at nighttime ($(3.39 \pm 1.34) \times 10^8$ particles h^{-1}) compared to those during the day ($(2.58 \pm 0.76) \times 10^8$ particles h^{-1}), which was associated with strong primary emissions, weak chemical processes, and low boundary layer height. The traffic emissions during rush hours also enhanced the deposition rate of hydrophobic particles. Based on a more explicit hygroscopicity measurement at RH = 98 %, this work provides insight into the impact of hygroscopicity on the deposition pattern of submicron particles in the HRT.

Although particle hygroscopicity was measured at a quite high RH (98 %), there is still a gap between the measurement conditions and the real HRT-conditions (RH = 99.5 %). The higher RH in the lower respiratory tract will lead to greater hygroscopic growth of particles. Since particle hygroscopicity may reduce the regional and total deposition doses, it is inferred that the higher RH in the lower HRT will further decrease the deposition dose. Therefore, developing advanced technology for measuring hygroscopicity in the real HRT-conditions will help to explore the influence of hygroscopicity on the particle deposition in the HRT more accurately. For instance, the HH-TDMA (Suda and Petters, 2013), the Leipzig Aerosol Cloud Interaction Simulator (Stratmann et al., 2004), the inverted streamwise-gradient cloud condensation nuclei counter (Ruehl et al., 2010), and the filter-based differential hygroscopicity analyzer (Mikhailov et al., 2011) have been used to determine particle hygroscopicity at RHs up to 99 %. In particular, Mikhailov and Vlasenko (2020) adopted a new method with in situ restructuring to minimize the influence of particle shape, and the RH was up to 99.6 %, with an RH measurement accuracy better than 0.4 %.

Due to the limited measurements and physiological parameters, some vital factors which may have an effect on the particle deposition in the HRT were not considered in this study, such as gender, exercise level, and the particle density. Besides, the deposition pattern of particles with diame-

ters larger than 1 µm was not discussed here due to the lack of measurements of the PNSD and hygroscopicity of coarse particles, while, as an important part of the ambient particle mass, coarse particles may also make a significant contribution to the particle deposition in the HRT (Fig. S7). The related research to find out the impact of particle hygroscopicity on the deposition mass dose of coarse particles ought to be carried out in the future.

Author contributions. ZW, JG, DvP, LZ, HH, and AW carried out the field observation and obtained data. RM, TZ, and YQ processed and analyzed the data. All authors discussed the results and contributed to the writing of this paper. RM prepared the paper, with contributions from all co-authors. ZW, AV, and MH further modified and improved the paper.

References

Asgharian, B., Hofmann, W., and Bergmann, R.: Particle Deposition in a Multiple-Path Model of the Human Lung, Aerosol Sci. Technol., 34, 332–339, https://doi.org/10.1080/02786820119122, 2001.

Avino, P., Scungio, M., Stabile, L., Cortellessa, G., Buonanno, G., and Manigrasso, M.: Second-hand aerosol from tobacco and electronic cigarettes: Evaluation of the smoker emission rates and doses and lung cancer risk of passive smokers and vapers, Sci. Total Environ., 642, 137–147, https://doi.org/10.1016/j.scitotenv.2018.06.059, 2018.

Baltensperger, U.: Urban and rural aerosol characterization of summer smog events during the PIPAPO field campaign in Milan, Italy, J. Geophys. Res., 107, 8193, https://doi.org/10.1029/2001jd001292, 2002.

Bian, Y. X., Zhao, C. S., Ma, N., Chen, J., and Xu, W. Y.: A study of aerosol liquid water content based on hygroscopicity measurements at high relative humidity in the North China Plain, Atmos. Chem. Phys., 14, 6417–6426, https://doi.org/10.5194/acp-14-6417-2014, 2014.

Birmili, W., Stratmann, F., and Wiedensohler, A.: Design of a DMA-based size spectrometer for a large particle size range and stable operation, J. Aerosol Sci., 30, 549–553, https://doi.org/10.1016/S0021-8502(98)00047-0, 1999.

Cao, L. X.: The geographical distribution of normal reference value of lung compliance and total lung capacity, Shaanxi Normal University, Xi'an, Shaanxi, China, 103 pp., 2009.

Chalvatzaki, E. and Lazaridis, M.: A dosimetry model of hygroscopic particle growth in the human respiratory tract, Air Qual. Atmos. Health, 11, 471–482, https://doi.org/10.1007/s11869-018-0555-7, 2018.

Chen, S., Wang, H., Lu, K., Zeng, L., Hu, M., and Zhang, Y.: The trend of surface ozone in Beijing from 2013 to 2019: Indications of the persisting strong atmospheric oxidation capacity, Atmos. Environ., 242, 117801, https://doi.org/10.1016/j.atmosenv.2020.117801, 2020.

Chen, Y., Ebenstein, A., Greenstone, M., and Li, H.: Evidence on the impact of sustained exposure to air pollution on life expectancy from China's Huai River policy, P. Natl. Acad. Sci. USA, 110, 12936–12941, https://doi.org/10.1073/pnas.1300018110, 2013.

Ching, J. and Kajino, M.: Aerosol mixing state matters for particles deposition in human respiratory system, Sci. Rep., 8, 8864, https://doi.org/10.1038/s41598-018-27156-z, 2018.

Correia, A. W., Pope, C. A., Dockery, D. W., Wang, Y., Ezzati, M., and Dominici, F.: Effect of air pollution control on life expectancy in the United States: an analysis of 545 U.S. counties for the period from 2000 to 2007, Epidemiology, 24, 23–31, https://doi.org/10.1097/EDE.0b013e3182770237, 2013.

Dockery, D. W., Pope, C. A., Xu, X., Spengler, J. D., Ware, J. H., Fay, M. E., Ferris, B. G., and Speizer, F. E.: An association between air pollution and mortality in six U.S. cities, N. Engl. J. Med., 329, 1753–1759, https://doi.org/10.1056/nejm199312093292401, 1993.

Donahue, N. M., Robinson, A. L., Trump, E. R., Riipinen, I., and Kroll, J. H.: Volatility and aging of atmospheric organic aerosol, Top. Curr. Chem., 339, 97–143, https://doi.org/10.1007/128_2012_355, 2014.

Duan, X., Zhao, X., Wang, B., Chen, Y., and Cao S.: Highlights of the Chinese Exposure Factors Handbook (Adults), edited by: Duan, X. L., Zhao, X. G., Wang, B. B., Chen, Y. T., and Gao,

S. Z., Science Press, Beijing, China, ISBN 978-7-03-042085-5, 2014.

Duan, X. L.: Highlights of the Chinese Exposure Factors Handbook (children), 1st edn., China Environment Publishing Group, Beijing, ISBN 978-7-5111-2812-6, China, 2016.

Farkas, A., Furi, P., Then, W., and Salma, I.: Effects of hygroscopic growth of ambient urban aerosol particles on their modelled regional and local deposition in healthy and COPD-compromised human respiratory system, Sci. Total Environ., 806, 151202, https://doi.org/10.1016/j.scitotenv.2021.151202, 2022.

Ferron, G. A.: The size of soluble aerosol particles as a function of the humidity of the air. Application to the human respiratory tract, J. Aerosol Sci., 8, 251–267, https://doi.org/10.1016/0021-8502(77)90045-3, 1977.

Gysel, M., McFiggans, G. B., and Coe, H.: Inversion of tandem differential mobility analyser (TDMA) measurements, J. Aerosol Sci., 40, 134–151, https://doi.org/10.1016/j.jaerosci.2008.07.013, 2009.

Haddrell, A. E., Davies, J. F., and Reid, J. P.: Dynamics of Particle Size on Inhalation of Environmental Aerosol and Impact on Deposition Fraction, Environ. Sci. Technol., 49, 14512–14521, https://doi.org/10.1021/acs.est.5b01930, 2015.

Haritash, A. K. and Kaushik, C. P.: Biodegradation aspects of polycyclic aromatic hydrocarbons (PAHs): a review, J. Hazard. Mater., 169, 1–15, https://doi.org/10.1016/j.jhazmat.2009.03.137, 2009.

Hart, M. C., Cook, C. D., and Orzalesi, M. M.: Relation between anatomic respiratory dead space and body size and lung volume, J. Appl. Physiol., 18, 519–522, https://doi.org/10.1152/jappl.1963.18.3.519, 1963.

Hennig, T., Massling, A., Brechtel, F. J., and Wiedensohler, A.: A Tandem DMA for highly temperature-stabilized hygroscopic particle growth measurements between 90 % and 98 % relative humidity, J. Aerosol Sci., 36, 1210–1223, https://doi.org/10.1016/j.jaerosci.2005.01.005, 2005.

Highwood, E. J. and Kinnersley, R. P.: When smoke gets in our eyes: the multiple impacts of atmospheric black carbon on climate, air quality and health, Environ. Int., 32, 560–566, https://doi.org/10.1016/j.envint.2005.12.003, 2006.

Hofmann, W.: Modelling inhaled particle deposition in the human lung – A review, J. Aerosol Sci., 42, 693–724, https://doi.org/10.1016/j.jaerosci.2011.05.007, 2011.

Hu, M., Peng, J., Sun, K., Yue, D., Guo, S., Wiedensohler, A., and Wu, Z.: Estimation of size-resolved ambient particle density based on the measurement of aerosol number, mass, and chemical size distributions in the winter in Beijing, Environ. Sci. Technol., 46, 9941–9947, https://doi.org/10.1021/es204073t, 2012.

Hussein, T., Londahl, J., Paasonen, P., Koivisto, A. J., Petaja, T., Hameri, K., and Kulmala, M.: Modeling regional deposited dose of submicron aerosol particles, Sci. Total Environ., 458–460, 140–149, https://doi.org/10.1016/j.scitotenv.2013.04.022, 2013.

Hussein, T., Saleh, S., dos Santos, V., Boor, B., Koivisto, A., and Löndahl, J.: Regional Inhaled Deposited Dose of Urban Aerosols in an Eastern Mediterranean City, Atmosphere, 10, 530, https://doi.org/10.3390/atmos10090530, 2019.

ICRP: Human respiratory tract model for radiological protection, ICRP Publ 66, Annals of ICRP, 24, 231, 1994.

Khlystov, A., Stanier, C., and Pandis, S. N.: An Algorithm for Combining Electrical Mobility and Aerodynamic Size Distributions Data when Measuring Ambient Aerosol Special Issue ofAerosol Science and Technologyon Findings from the Fine Particulate Matter Supersites Program, Aerosol Sci. Technol., 38, 229–238, https://doi.org/10.1080/02786820390229543, 2004.

Kim, K. H., Jahan, S. A., Kabir, E., and Brown, R. J.: A review of airborne polycyclic aromatic hydrocarbons (PAHs) and their human health effects, Environ. Int., 60, 71–80, https://doi.org/10.1016/j.envint.2013.07.019, 2013.

Kristensson, A., Rissler, J., Löndahl, J., Johansson, C., and Swietlicki, E.: Size-Resolved Respiratory Tract Deposition of Sub-Micrometer Aerosol Particles in a Residential Area with Wintertime Wood Combustion, Aerosol Air Qual. Res., 13, 24–35, https://doi.org/10.4209/aaqr.2012.07.0194, 2013.

Li, X., Yan, C., Patterson, R. F., Zhu, Y., Yao, X., Zhu, Y., Ma, S., Qiu, X., Zhu, T., and Zheng, M.: Modeled deposition of fine particles in human airway in Beijing, China, Atmos. Environ., 124, 387–395, https://doi.org/10.1016/j.atmosenv.2015.06.045, 2016.

Liu, P., Song, M., Zhao, T., Gunthe, S. S., Ham, S., He, Y., Qin, Y. M., Gong, Z., Amorim, J. C., Bertram, A. K., and Martin, S. T.: Resolving the mechanisms of hygroscopic growth and cloud condensation nuclei activity for organic particulate matter, Nat. Commun., 9, 4076, https://doi.org/10.1038/s41467-018-06622-2, 2018.

Londahl, J., Massling, A., Pagels, J., Swietlicki, E., Vaclavik, E., and Loft, S.: Size-resolved respiratory-tract deposition of fine and ultrafine hydrophobic and hygroscopic aerosol particles during rest and exercise, Inhal. Toxicol., 19, 109–116, https://doi.org/10.1080/08958370601051677, 2007.

Londahl, J., Massling, A., Swietlicki, E., Brauner, E. V., Ketzel, M., Pagels, J., and Loft, S.: Experimentally Determined Human Respiratory Tract Deposition of Airborne Particles at a Busy Street, Environ. Sci. Technol., 43, 4659–4664, https://doi.org/10.1021/es803029b, 2009.

Lyu, Y., Guo, H., Cheng, T., and Li, X.: Particle Size Distributions of Oxidative Potential of Lung-Deposited Particles: Assessing Contributions from Quinones and Water-Soluble Metals, Environ. Sci. Technol., 52, 6592–6600, https://doi.org/10.1021/acs.est.7b06686, 2018.

Man, R. Q.: Regional and total deposition doses of submicron particles for different age groups of Chinese population, Dryad Digital Repository [data set], https://doi.org/10.5061/dryad.h18931zq2, 2022.

Manigrasso, M., Buonanno, G., Fuoco, F. C., Stabile, L., and Avino, P.: Aerosol deposition doses in the human respiratory tree of electronic cigarette smokers, Environ. Pollut., 196, 257–267, https://doi.org/10.1016/j.envpol.2014.10.013, 2015.

Manigrasso, M., Vernale, C., and Avino, P.: Traffic aerosol lobar doses deposited in the human respiratory system, Environ. Sci. Pollut. Res. Int., 24, 13866–13873, https://doi.org/10.1007/s11356-015-5666-1, 2017.

Mauderly, J. L. and Chow, J. C.: Health effects of organic aerosols, Inhal. Toxicol., 20, 257–288, https://doi.org/10.1080/08958370701866008, 2008.

Mikhailov, E. F. and Vlasenko, S. S.: High-humidity tandem differential mobility analyzer for accurate determination of aerosol hygroscopic growth, microstructure, and activity coefficients over a wide range of relative humidity, Atmos. Meas. Tech., 13, 2035–2056, https://doi.org/10.5194/amt-13-2035-2020, 2020.

Mikhailov, E. F., Merkulov, V. V., Vlasenko, S. S., Ryshkevich, T. I., and Poschl, U. J.: Filter-based differential hygroscopicity analyzer of aerosol particles, Izv. Atmos. Ocean. Phy., 47, 747–759, https://doi.org/10.1134/s0001433811060107, 2011.

Mitsakou, C., Housiadas, C., Eleftheriadis, K., Vratolis, S., Helmis, C., and Asimakopoulos, D.: Lung deposition of fine and ultrafine particles outdoors and indoors during a cooking event and a no activity period, Indoor Air, 17, 143–152, https://doi.org/10.1111/j.1600-0668.2006.00464.x, 2007.

Oberdorster, G.: Pulmonary effects of inhaled ultrafine particles, Int. Arch. Occup. Environ. Health, 74, 1–8, https://doi.org/10.1007/s004200000185, 2001.

Petters, M. D. and Kreidenweis, S. M.: A single parameter representation of hygroscopic growth and cloud condensation nucleus activity, Atmos. Chem. Phys., 7, 1961–1971, https://doi.org/10.5194/acp-7-1961-2007, 2007.

Pope III, C. A., and Dockery, D. W.: Air pollution and life expectancy in China and beyond, P. Natl. Acad. Sci. USA, 110, 12861–12862, https://doi.org/10.1073/pnas.1310925110, 2013.

Pope III, C. A., Ezzati, M., and Dockery, D. W.: Fine-Particulate Air Pollution and Life Expectancy in the United States, N. Engl. J. Med., 360, 376–386, https://doi.org/10.1056/NEJMsa0805646, 2009.

Raes, F., Dingenen, R. V., Vignati, E., Wilson, J., Putaud, J.-P., Seinfeld, J. H., and Adams, P.: Formation and cycling of aerosols in the global troposphere, Atmos. Environ., 34, 4215–4240, https://doi.org/10.1016/S1352-2310(00)00239-9, 2000.

Rudich, Y., Donahue, N. M., and Mentel, T. F.: Aging of organic aerosol: bridging the gap between laboratory and field studies, Annu. Rev. Phys. Chem., 58, 321–352, https://doi.org/10.1146/annurev.physchem.58.032806.104432, 2007.

Ruehl, C. R., Chuang, P. Y., and Nenes, A.: Aerosol hygroscopicity at high (99 to 100 %) relative humidities, Atmos. Chem. Phys., 10, 1329–1344, https://doi.org/10.5194/acp-10-1329-2010, 2010.

Stocks, J. and Quanjer, P. H.: Reference values for residual volume, functional residual capacity and total lung capacity. ATS Workshop on Lung Volume Measurements. Official Statement of The European Respiratory Society, Eur. Respir. J., 8, 492–506, https://doi.org/10.1183/09031936.95.08030492, 1995.

Stratmann, F., Kiselev, A., Wurzler, S., Wendisch, M., Heintzenberg, J., Charlson, R. J., Diehl, K., Wex, H., and Schmidt, S.: Laboratory studies and numerical simulations of cloud droplet formation under realistic supersaturation conditions, J. Atmos. Ocean. Tech., 21, 876–887, https://doi.org/10.1175/1520-0426(2004)021<0876:Lsanso>2.0.Co;2, 2004.

Suda, S. R. and Petters, M. D.: Accurate Determination of Aerosol Activity Coefficients at Relative Humidities up to 99 % Using the Hygroscopicity Tandem Differential Mobility Analyzer Technique, Aerosol Sci. Tech., 47, 991–1000, https://doi.org/10.1080/02786826.2013.807906, 2013.

Swietlicki, E., Hansson, H. C., Hameri, K., Svenningsson, B., Massling, A., McFiggans, G., McMurry, P. H., Petaja, T., Tunved, P., Gysel, M., Topping, D., Weingartner, E., Baltensperger, U., Rissler, J., Wiedensohler, A., and Kulmala, M.: Hygroscopic properties of submicrometer atmospheric aerosol particles measured with H-TDMA instruments in various environments – a

review, Tellus B, 60, 432–469, https://doi.org/10.1111/j.1600-0889.2008.00350.x, 2008.

Tan, T., Guo, S., Wu, Z., He, L., Huang, X., and Hu, M.: Impact of aging process on atmospheric black carbon aerosol properties and climate effects, Chin. Sci. Bull., 65, 4235–4250, https://doi.org/10.1360/tb-2020-0745, 2020.

Tan, Z., Hofzumahaus, A., Lu, K., Brown, S. S., Holland, F., Huey, L. G., Kiendler-Scharr, A., Li, X., Liu, X., Ma, N., Min, K. E., Rohrer, F., Shao, M., Wahner, A., Wang, Y., Wiedensohler, A., Wu, Y., Wu, Z., Zeng, L., Zhang, Y., and Fuchs, H.: No Evidence for a Significant Impact of Heterogeneous Chemistry on Radical Concentrations in the North China Plain in Summer 2014, Environ. Sci. Technol., 54, 5973–5979, https://doi.org/10.1021/acs.est.0c00525, 2020.

Topping, D. O. and McFiggans, G.: Tight coupling of particle size, number and composition in atmospheric cloud droplet activation, Atmos. Chem. Phys., 12, 3253–3260, https://doi.org/10.5194/acp-12-3253-2012, 2012.

Varghese, S. K. and Gangamma, S.: Particle deposition in human respiratory system: deposition of concentrated hygroscopic aerosols, Inhal. Toxicol., 21, 619–630, https://doi.org/10.1080/08958370802380792, 2009.

Voliotis, A. and Samara, C.: Submicron particle number doses in the human respiratory tract: implications for urban traffic and background environments, Environ. Sci. Pollut. Res. Int., 25, 33724–33735, https://doi.org/10.1007/s11356-018-3253-y, 2018.

Voliotis, A., Bezantakos, S., Besis, A., Shao, Y., and Samara, C.: Mass dose rates of particle-bound organic pollutants in the human respiratory tract: Implications for inhalation exposure and risk estimations, Int. J. Hyg. Environ. Health, 234, 113710, https://doi.org/10.1016/j.ijheh.2021.113710, 2021.

Vu, T., Delgado-Saborit, J., and Harrison, R.: A review of hygroscopic growth factors of submicron aerosols from different sources and its implication for calculation of lung deposition efficiency of ambient aerosols, Air Qual. Atmos. Health, 8, 429–440, https://doi.org/10.1007/s11869-015-0365-0, 2015.

Vu, T. V., Zauli-Sajani, S., Poluzzi, V., and Harrison, R. M.: Factors controlling the lung dose of road traffic-generated sub-micrometre aerosols from outdoor to indoor environments, Air Qual. Atmos. Health, 11, 615–625, https://doi.org/10.1007/s11869-018-0568-2, 2018.

Wang, H., Yin, P., Fan, W., Wang, Y., Dong, Z., Deng, Q., and Zhou, M.: Mortality Risk Associated with Short-Term Exposure to Particulate Matter in China: Estimating Error and Implication, Environ. Sci. Technol., 55, 1110–1121, https://doi.org/10.1021/acs.est.0c05095, 2021.

Wang, L., Zheng, X., Stevanovic, S., Wu, X., Xiang, Z., Yu, M., and Liu, J.: Characterization particulate matter from several Chinese cooking dishes and implications in health effects, J. Environ. Sci.-China, 72, 98–106, https://doi.org/10.1016/j.jes.2017.12.015, 2018.

Wang, T., Du, Z., Tan, T., Xu, N., Hu, M., Hu, J., and Guo, S.: Measurement of aerosol optical properties and their potential source origin in urban Beijing from 2013–2017, Atmos. Environ., 206, 293–302, https://doi.org/10.1016/j.atmosenv.2019.02.049, 2019.

Wang, X., Shen, X. J., Sun, J. Y., Zhang, X. Y., Wang, Y. Q., Zhang, Y. M., Wang, P., Xia, C., Qi, X. F., and Zhong, J. T.: Size-resolved hygroscopic behavior of atmospheric aerosols during heavy aerosol pollution episodes in

Beijing in December 2016, Atmos. Environ., 194, 188–197, https://doi.org/10.1016/j.atmosenv.2018.09.041, 2018.

Wex, H., Petters, M. D., Carrico, C. M., Hallbauer, E., Massling, A., McMeeking, G. R., Poulain, L., Wu, Z., Kreidenweis, S. M., and Stratmann, F.: Towards closing the gap between hygroscopic growth and activation for secondary organic aerosol: Part 1 – Evidence from measurements, Atmos. Chem. Phys., 9, 3987–3997, https://doi.org/10.5194/acp-9-3987-2009, 2009.

Wiedensohler, A., Birmili, W., Nowak, A., Sonntag, A., Weinhold, K., Merkel, M., Wehner, B., Tuch, T., Pfeifer, S., Fiebig, M., Fjäraa, A. M., Asmi, E., Sellegri, K., Depuy, R., Venzac, H., Villani, P., Laj, P., Aalto, P., Ogren, J. A., Swietlicki, E., Williams, P., Roldin, P., Quincey, P., Hüglin, C., Fierz-Schmidhauser, R., Gysel, M., Weingartner, E., Riccobono, F., Santos, S., Grüning, C., Faloon, K., Beddows, D., Harrison, R., Monahan, C., Jennings, S. G., O'Dowd, C. D., Marinoni, A., Horn, H.-G., Keck, L., Jiang, J., Scheckman, J., McMurry, P. H., Deng, Z., Zhao, C. S., Moerman, M., Henzing, B., de Leeuw, G., Löschau, G., and Bastian, S.: Mobility particle size spectrometers: harmonization of technical standards and data structure to facilitate high quality long-term observations of atmospheric particle number size distributions, Atmos. Meas. Tech., 5, 657–685, https://doi.org/10.5194/amt-5-657-2012, 2012.

Wu, Z. J., Poulain, L., Henning, S., Dieckmann, K., Birmili, W., Merkel, M., van Pinxteren, D., Spindler, G., Müller, K., Stratmann, F., Herrmann, H., and Wiedensohler, A.: Relating particle hygroscopicity and CCN activity to chemical composition during the HCCT-2010 field campaign, Atmos. Chem. Phys., 13, 7983–7996, https://doi.org/10.5194/acp-13-7983-2013, 2013.

Wu, Z. J., Zheng, J., Shang, D. J., Du, Z. F., Wu, Y. S., Zeng, L. M., Wiedensohler, A., and Hu, M.: Particle hygroscopicity and its link to chemical composition in the urban atmosphere of Beijing, China, during summertime, Atmos. Chem. Phys., 16, 1123–1138, https://doi.org/10.5194/acp-16-1123-2016, 2016.

Wu, Z., Zheng, J., Wang, Y., Shang, D., Du, Z., Zhang, Y., and Hu, M.: Chemical and physical properties of biomass burning aerosols and their CCN activity: A case study in Beijing, China, Sci. Total Environ., 579, 1260–1268, https://doi.org/10.1016/j.scitotenv.2016.11.112, 2017a.

Wu, Z. J., Ma, N., Größ, J., Kecorius, S., Lu, K. D., Shang, D. J., Wang, Y., Wu, Y. S., Zeng, L. M., Hu, M., Wiedensohler, A., and Zhang, Y. H.: Thermodynamic properties of nanoparticles during new particle formation events in the atmosphere of North China Plain, Atmos. Res., 188, 55–63, https://doi.org/10.1016/j.atmosres.2017.01.007, 2017b.

Youn, J. S., Csavina, J., Rine, K. P., Shingler, T., Taylor, M. P., Saez, A. E., Betterton, E. A., and Sorooshian, A.: Hygroscopic Properties and Respiratory System Deposition Behavior of Particulate Matter Emitted by Mining and Smelting Operations, Environ. Sci. Technol., 50, 11706–11713, https://doi.org/10.1021/acs.est.6b03621, 2016.

Zhang, Y., Zhang, S., Huang, C., Huang, K., Gong, Y., and Gan, Q.: Diurnal variations of the planetary boundary layer height estimated from intensive radiosonde observations over Yichang, China, Sci. China Technol. Sc., 57, 2172–2176, https://doi.org/10.1007/s11431-014-5639-5, 2014.

Zong, T., Wang, H., Wu, Z., Lu, K., Wang, Y., Zhu, Y., Shang, D., Fang, X., Huang, X., He, L., Ma, N., Gross, J., Huang, S., Guo, S., Zeng, L., Herrmann, H., Wiedensohler, A., Zhang, Y., and Hu, M.: Particle hygroscopicity inhomogeneity and its impact on reactive uptake, Sci. Total Environ., 811, 151364, https://doi.org/10.1016/j.scitotenv.2021.151364, 2021.

Zhu, G. J.: Physiological constants and psychological status of Chinese population, Peking Union Medical College, Beijing, China, ISBN 7-81072-774-5, 2006.